Cite this: Faraday Discuss., 2013, 164, 57

PAPER

Potential-dependent single molecule blinking dynamics for flavin adenine dinucleotide covalently immobilized in zero-mode waveguide array of working electrodes

Jing Zhao, Lawrence P. Zaino IIIb and Paul W. Bohn*ab

Received 12th February 2013, Accepted 6th March 2013

DOI: 10.1039/c3fd00013c

Single molecules exhibit a set of behaviors that are characteristic and distinct from larger ensembles. Blinking is one such behavior that involves episodic transitions between luminescent and dark states. In addition to the common blinking mechanisms, flavin adenine dinucleotide (FAD), a cofactor in many common redox enzymes, exhibits blinking by cycling between a highly fluorescent oxidized state and a dark reduced state. In contrast to its behavior in flavoenzymes, where the transitions are coupled to chemical redox events, here we study single FAD molecules that are chemically immobilized to the Au region of a zero-mode waveguide (ZMW) array through a pyrroloquinoline quinone (PQQ) linker. In this structure, the Au functions both to confine the optical field in the ZMW and as the working electrode in a potentiostatically controlled 3-elecrode system, thus allowing potential-dependent blinking to be studied in single FAD molecules. The subset of ZMW nanopores housing a single molecule were identified statistically, and these were subjected to detailed study. Using equilibrium potential, E_{eq} , values determined from macroscopic planar Au electrodes, single molecule blinking behavior was characterized at potentials $E < E_{\rm eq}$, $E \sim E_{\rm eq}$, and $E > E_{\rm eq}$. The probability of observing a reduced (oxidized) state is observed to increase (decrease) as the potential is scanned cathodic of E_{eq} . This is understood to reflect the potential-dependent probability of electron transfer for single FAD molecules. Furthermore, the observed transition rate reaches a maximum near E_{eq} and decreases to either anodic or cathodic values, as expected, since the rate is dependent on having significant probabilities for both redox states, a condition that is obtained only near E_{eq} .

Introduction

The effects of confinement on chemical reactivity are of intense interest, however these effects are difficult to study at the ensemble level where the

^aDepartment of Chemical and Biomolecular Engineering, University of Notre Dame, Notre Dame, IN 46556, USA. E-mail: pbohn@nd.edu

^bDepartment of Chemistry and Biochemistry, University of Notre Dame, Notre Dame, IN 46556, USA

magnitude—and even sign—of the effect may vary from system to system and may be confounded by extraneous physical and chemical characteristics of the immediate environment.¹⁻⁷ One problem in obtaining consistent results is developing a robust experimental protocol that allows the fundamental biophysical/chemical parameters to be isolated from confounding effects. In this regard, zero mode waveguides (ZMWs) offer some unique advantages. ZMWs were initially used to study single binding/catalysis events for systems with µM ligand concentrations.8-11 Consisting of zeptoliter (1 zL = 10^{-21} L) volume cylindrical nanopores in an opaque film (typically Al^{12,13}), ZMWs serve to confine the electromagnetic field inside the nanocylinder, thus enhancing the signal-to-background ratio in spectroscopic experiments. Owing to their small volume, excellent optical confinement, spatial localization, and signal enhancement, ZMWs have been used to study single molecule DNA sequencing,14 protein-protein interactions, 15 and plasma membrane dynamics. 10,11,16 Furthermore, spectroscopy can be accomplished either by imaging a large number of parallel ZMWs simultaneously, 12,13,15 or by fluorescence correlation. 16,17

Previously, we constructed Au-based ZMWs for studies of the enzyme monomeric sarcosine oxidase (MSOX),18 a flavoenzyme in which the flavin adenine dinucleotide (FAD) cofactor exhibits blinking by cycling between a highly fluorescent oxidized state and a dark reduced state. In these experiments electron transfer was constrained to occur between solution-phase substrate and MSOX immobilized to the SiO₂ floor in the interior of the ZMW. The resulting observation of single molecule fluorescence signatures correlated to redox events raises the possibility of using the same strategy to observe direct heterogeneous electron transfer from metallic electrodes to single redox-active molecules. Thus, in contrast to its behavior in flavoenzymes, where the transitions are coupled to chemical redox events, here we study single FAD molecules that are chemically immobilized to a Au working electrode in a zero-mode waveguide (ZMW) array structure through a pyrroloquinoline quinone (PQQ) linker.19

Single molecule electrochemistry has been studied since the pioneering experiments by Bard and coworkers utilizing a recessed SECM tip to trap electroactive species, thus amplifying the electrochemical signal above the background by redox cycling and realizing the limit of electrochemical sample size. 20,21 Although these and subsequent experiments have observed the electrochemical behavior of single molecules, observing single electron transfer events is a much more challenging objective. To approach this goal, Lemay and coworkers used lithographically-prepared nanoelectrodes to observe single enzyme electrochemistry in structures producing fA-scale currents commensurate with the electron transfer activity of ~10 molecules.22,23

In trapped molecule experiments, assuming that the electrode kinetics are not rate-limiting, the electron transfer rate is given by an inverse transit time

$$\tau^{-1} = \frac{2D}{\langle x^2 \rangle} \tag{1}$$

where *D* is the diffusion coefficient and *x* is the separation between electrodes. In contrast, single molecule spectroelectrochemistry produces emitting states that, as long as they can be physically retained in the focal volume, turnover at a rate,

$$N = \frac{\sigma \phi_{\rm F} P}{Ahv} \tag{2}$$

where the turnover rate, N, is determined by the absorption cross-section, σ , and source flux, $P/Ah\nu$, as modified by the fluorescence quantum yield, $\phi_{\rm F}$. In trapped molecule electrochemistry with $D \sim 10^{-5} \text{ cm}^2 \text{ s}^{-1}$ and $d \sim 10 \text{ nm}$, it is possible to achieve redox cycling rates of the order $\sim 10^7$ s⁻¹. In contrast, single molecule fluorescence, limited ultimately by photobleaching, can achieve turnover values as high as $10^4 \, \mathrm{s}^{-1}$. Furthermore, by careful manipulation of the optical environment, using total internal reflection excitation for example, it is possible to drastically reduce the background, so that single molecule fluorescence can be observed at S/N ratios as large as 100.24,25 Thus, if redox events can be coupled to the probability that a chromophore emits, then excited state cycling can be used to replace redox cycling to identify and locate electron transfer events.

Recent studies have demonstrated amplification of electron transfer reactions by spectroscopic monitoring. 22,26-28 For example, the conversion between a fluorescent and non-fluorescent state can be monitored while modulating the potential of the cell. Barbara, Bard and coworkers showed that single molecule spectroelectrochemistry can be performed on polymer films coated on indium tin oxide with total internal reflectance fluorescence (TIRF) microscopy.28 Spectroelectrochemical studies of single molecules have also been performed by single molecule spectroscopy under potential control, using confocal microscopy to monitor a focal volume adjacent to the working electrode surface. 27,29

Flavoenzymes, containing a FAD cofactor based on the isoalloxazine chromophore, have been a particular target of single molecule fluorescence studies, 30,31 because the molecule is highly fluorescent in the oxidized state and dark in the reduced state.³² Previous research from this laboratory used ZMWs to study the dynamics of single MSOX enzymes, which contain a FAD cofactor.18 Thus, the combination of ZMWs (to isolate single FAD molecules and reduce the spectroscopic background) with a Au cladding (used as a working electrode to control the electrochemical potential) provides an ideal platform to investigate the relationship between single molecule fluorescence and single electron transfer events. In addition, because an array of ZMWs is imaged simultaneously, multiple single FAD molecules can be studied in parallel.

Experimental

ZMW fabrication

Zero-mode waveguides were fabricated by a procedure similar to that reported previously. 18 Briefly, a ~170 μm thick fused silica coverslip was cleaned using freshly prepared piranha solution $(3:1 \text{ H}_2\text{SO}_4:\text{H}_2\text{O}_2 - Caution: piranha is an)$ extremely aggressive oxidant and should be used with great care), rinsed with copious amounts of a series of solvents, including deionized (DI) water, acetone, and isopropanol, followed by a final DI water rinse, then dried using N2. The substrate was then coated with a thin $(d \le 100 \text{ nm})$ layer of Au by thermal evaporation at \sim 0.1 nm s⁻¹. The modified 1 cm \times 1 cm area was then coated with 10 nm Cr to passivate the top surfaces against subsequent organomercaptan selfassembly. All evaporated film thicknesses were measured by a quartz crystal filmthickness monitor. A dual-source focused ion beam (FIB) instrument (Helios Nanolab 600, FEI Corp.) was used for milling and characterization. ZMWs were patterned in a 70 μ m \times 70 μ m square array with a lattice constant of 2 μ m by FIB ion milling. The diameters of the individual nanopores constituting the ZMWs

were chosen to be between 60 and 150 nm. Finally, after FAD immobilization polydimethylsiloxane (PDMS) wells were placed on the coverslip to isolate individual arrays for convenient sample application.

FAD immobilization

The Au electrodes were cleaned by boiling in 2M KOH for 1 h followed by rinsing with DI water. They were stored in concentrated H2SO4 and then soaked for 10 min in concentrated HNO3 and rinsed again with DI water. The clean Au electrodes were then soaked in a solution of 0.05 M cystamine in DI water for 1 h and then rinsed thoroughly with DI water after emersion. The cystamine-modified Au-electrodes were incubated in 3 mM PQQ in 0.1 M pH 7.2 HEPES-buffer in the presence of 5 mM 1-ethyl-3-[3-dimethylaminopropyl]carbodiimide hydrochloride (EDC) for 2 h. The POO-functionalized electrodes were subsequently reacted with 1 mM 3-aminophenylboronic acid in 0.1 M pH 7.2 HEPES buffer in the presence of 5 mM EDC for 2 h, followed by rinsing with DI water. The resulting electrode was treated with FAD, typically at a concentration of 10-30 nM in 0.1 M pH 7.0 phosphate buffer for 2 h at room temperature and then overnight at 4 °C followed by washing with DI water. The concentration was determined to yield an optimal distribution of ZMWs occupied with single FAD molecules.

Electrochemical measurements

Electrochemical measurements were performed using an electrochemical analyzer (Reference 600, Gamry Instruments). The measurements were carried out at an ambient temperature using FAD modified Au as a working electrode, an unmodified Au film as a counter electrode, and a saturated Ag/AgCl reference electrode. For CV measurements, FAD immobilization was accomplished as above, but using 1 mM FAD in 0.1 M pH 7.0 phosphate buffer to prepare macroscopic FAD-derivatized planar Au working electrodes. Cyclic voltammetry was performed in 0.1 M pH 7.2 phosphate buffer at 50 mV s $^{-1}$.

Fluorescence measurements

Fluorescence measurements were performed on an Olympus IX71 wide-field epiillumination microscope. Laser radiation at 488 nm was reflected into the microscope and defocused to illuminate an area \sim 70 μ m \times 70 μ m on the fused silica substrate side of the ZMW sample to directly excite single FAD fluorescence in individual ZMW nanopores. The resulting fluorescence was collected by the same oil immersion objective (100 \times , 1.4 NA) and projected onto a 512 \times 512 pixel Andor charge-coupled device (CCD) camera (Andor Technology) with a $1.5 \times$ tube lens, achieving a net magnification of $150 \times$. A dichroic mirror (Chroma Z488RDC) and an emission filter (Chroma HQ525/50m) were used to discriminate against scattered excitation radiation. Sequential image frames were acquired with 50 ms exposure for subsequent data analysis using Igor (Wavemetrics) software. Movies were processed by first identifying individual localized fluorescence regions of interest (ROIs), the intensity of which was obtained by integrating the signal over a 6×6 pixel area. Temporal fluorescence intensity trajectories were then calculated from each ROI for subsequent statistical analysis. Potential-dependent fluorescence trajectories were obtained by applying the stated potential vs.

Ag/AgCl to the entire ZMW array in 0.1 M pH 7.2 phosphate buffer. All solutions were sparged with N₂ prior to ZMW fluorescence experiments to remove O₂.

Results and discussion

Construction of electrochemical ZMW arrays

To obtain fluorescence readout of single molecule electron transfer events, it is necessary to isolate single electroactive molecules so that they may be addressed both electrochemically and optically. The strategy used here involves the fabrication of controlled-potential ZMW structures in which a subpopulation of ZMW nanopores contain a single molecule—the rest containing either zero or multiple molecules, viz. Fig. 1. The ZMWs containing single FAD molecules are identified by standard statistical tests applied to the fluorescence trajectories from all ZMWs.^{33,34} The optical intensity through a cylindrical zero-mode waveguide can be expressed as

$$I(z) = \exp\left[-2z\sqrt{\frac{1}{\lambda_{\rm c}^2} - \frac{1}{\lambda_{\rm m}^2}}\right] \tag{3}$$

where $\lambda_c = 1.7d$ is the cut-off wavelength, d is the diameter for a cylindrical ZMW, and $\lambda_{\rm m}$ is the wavelength in the core medium, 367 nm in the present experiment. Thus, the nominal observation volume, i.e. the volume in which the radiation field is contained, for a 100 nm diameter ZMW is ~125 zL. Although the lightblocking efficiency of the Au is lower than the commonly used Al, Au was used to construct ZMWs in these experiments because Au enables a wide range of selfassembly surface chemistry which can be used to synthesize the immobilized

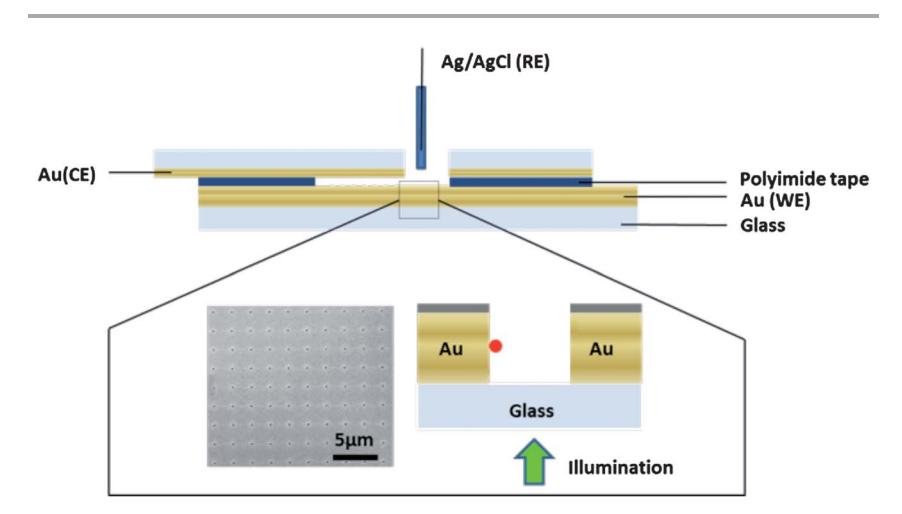


Fig. 1 Schematic (side view) diagram of the ZMW-electrochemical cell made between Au-coated fused silica containing ZMW working electrode (WE) arrays and a Au-coated coverslip counter electrode (CE). The structure uses a macroscopic Ag/AgCl reference electrode (RE). Each square ZMW array consists of \sim 1000 ZMWs with 2 μ m period. The diameter of the ZMW nanopores is 100 nm. The laser illuminates the device from the fused silica side. (Expanded view) Left: SEM image showing a portion of the ZMW array. Right: Schematic diagram showing a typical location of an individual FAD/FADH2 molecule (red) immobilized on the Au WE.

electroactive species. In this work, FAD molecules are immobilized on the Au sidewalls of the ZMW nanopores—rather than the fused silica bottom surfaces—specifically to access heterogeneous electron transfer processes. However, as indicated by eqn (3), there is a dispersion in the excitation intensity among single molecules in different ZMWs. Those near the bottom of the ZMWs are more strongly excited due to the intensity decay along the *z*-axis of the ZMWs.

In these experiments, uniform ZMW arrays containing $\sim 10^3$ ZMWs were prepared by fast FIB milling to allow parallel multiplexed observation of multiple single molecules at the same applied potential. Assuming a Poisson distribution governs molecular occupancy of the ZMWs, the concentration of FAD was adjusted in the range 10-30 nM (depending on the ZMW diameter) to optimize the yield of ZMWs with single FAD chromophores bound to the Au sidewalls within the observation volume. To ensure that electrochemically addressable immobilized fluorescent FAD were obtained, FAD molecules were isolated on the surface of the Au sidewalls using an organothiol-directed 3-step synthesis shown in Scheme 1. Following the molecular logic gate work of Pita and Katz,19 the Au surface was prepared with a self-assembled monolayer presenting a terminal amine for derivatization with PQQ and subsequently with m-aminophenylboronic acid, both of which were carried out with EDC coupling chemistry. 35,36 PQO has three possible sites for amide coupling, but these experiments were carried out without control over the three possible regioisomers. Finally, FAD was immobilized by coupling to the surface phenylboronic ester through the sugar moiety. The efficacy of this immobilization strategy was tested on macroscopic planar Au surfaces. The resulting structures demonstrate that the linker is competent to support electron transfer as supported by cyclic voltammetry and differential pulse voltammetry, the latter yielding a robust measure of surface coverage of 9.3×10^{-11} mol cm⁻², in good agreement with Pita and Katz. ¹⁹ Binding of FAD on large scale planar Au resulted in a peak (E = -0.48 V vs. Ag/AgCl) corresponding to the redox process for surface immobilized FAD. This peak position was used in subsequent ZMW electrochemistry experiments as an estimate of the position of the single molecule equilibrium potential, $E_{eq} = -0.48 \text{ V } vs. \text{ Ag/AgCl.}$

Scheme 1

In any surface immobilization scheme, non-specific adsorption is a potential problem. In addition, the existence of solution-phase FAD molecules diffusing in or out of the observation volume would also complicate recognition of the FAD-FADH₂ transitions occurring on Au sidewalls. To evaluate the influence of these potential sources of interference, the fluorescence from a ZMW array filled with free FAD solution was monitored in the absence of POO surface linker molecules using the same concentration as that used for immobilization, i.e. 30 nM. Under these conditions, the intensity of non-specifically adsorbed and freely diffusing FAD was found to be negligible in comparison to that of single molecules of covalently attached FAD within the same temporal observation window. Therefore, interferences from non-specific adsorption and desorption of FAD and from freely diffusing FAD were neglected.

Representative single molecule emission behavior

The wide-field imaging strategy implemented here allows multiplexed real-time observation of multiple ZMW nanopores, each containing a single FAD molecule. FAD derivatization solution concentrations in the range 10-30 nM were found to vield acceptable single molecule occupancies, although structures prepared from 10 nM FAD solutions were found to minimize contributions from multiply occupied ZMWs. To distinguish single FAD molecules from multiple molecules, fluorescence levels corresponding to all potential ROIs, i.e. ZMWs, were plotted as intensity histograms. The fluorescence levels of FAD molecules immobilized in the ZMW were determined by comparison with the fluorescence intensity of ZMWs containing zero molecules, i.e. ZMWs exhibiting no jumps in fluorescence level during the entire trajectory, which were regarded as defining the background. These ZMW ROIs produced intensity distributions with a single peak at the lowest count level for 50 ms acquisition, i.e. \sim 5500 counts, allowing this level to be assigned to ZMWs containing zero molecules. ZMWs with episodic fluorescence intensities exceeding this background were assigned to occupancies $n \ge 1$. Analysis of the integrated fluorescence intensity histograms in these frames frequently yielded peaks at multiple positions, as shown in Fig. 2, but with variable intensities. The next two discrete histogram peaks can be assigned to n=1and 2, respectively. Variable intensity distributions from the same number of molecules in different ZMW nanopores is attributed to differential positioning of the fluorescent FAD molecules relative to the ZMW excitation field and to different orientations of the chromophores relative to the surface. Increased FAD loading was also observed with larger ZMW diameters.

In addition to the histograms, typical fluorescence intensity trajectories of single FAD molecules, obtained without potential control, exhibit blinking and eventual photobleaching. Under the same laser excitation and solution conditions used to acquire potential-dependent data, control experiments (without potential control) show that the photobleaching times of immobilized FAD molecules, $\tau_{photobleach} = 110 \pm 70$ s, are much longer than the average on-time duration (ranging from a few hundred milliseconds to a few seconds) in the ZMW fluorescence trajectories obtained under potential control. Also, open-circuit FAD measurements yield an on-time distribution that decays exponentially with time constant $\tau_{\text{blink}} = 9.7 \pm 0.6$ s, the timescale of which is compared below to the temporal characteristics of blinking under potential control. Given the much

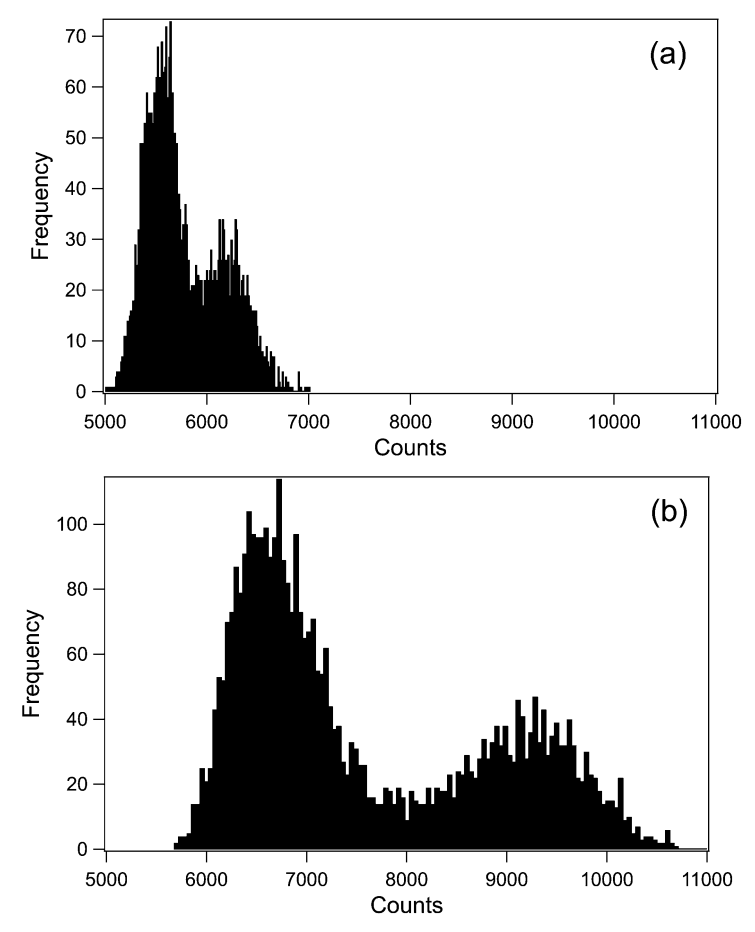


Fig. 2 Representative histograms of 6 min trajectories illustrating the relationship of the discrete fluorescence levels to molecular occupancy. (a) Single molecule occupancy exhibits an intensity peak near that of the background, ~5500 counts, and a single distinct peak at higher intensity. (b) Multiple molecule occupancy exhibits peaks at single molecule levels and higher.

longer time scale of photobleaching compared to potential-dependent blinking, this phenomenon can be safely neglected in analysis of potential-dependent single molecule fluorescence behavior. Furthermore, the characteristic blinking behavior under potential control can readily be distinguished from the open circuit behavior, so the intrinsic blinking does not confound interpretation of the potential-dependent single molecule behavior.

Potential dependent single molecule intensity distributions

When applying a potential to the ZMW working electrode array, movies of ZMW single molecule fluorescence show repetitive stochastic bursts at frequencies that are potential dependent. Typical data shown in Fig. 3 all exhibit stochastic two-state off-on signals, but the on- and off-time distributions vary dramatically as a function of potential. The digital, two-state nature of these fluorescence trajectories is consistent with the interpretation that each burst comes from a single

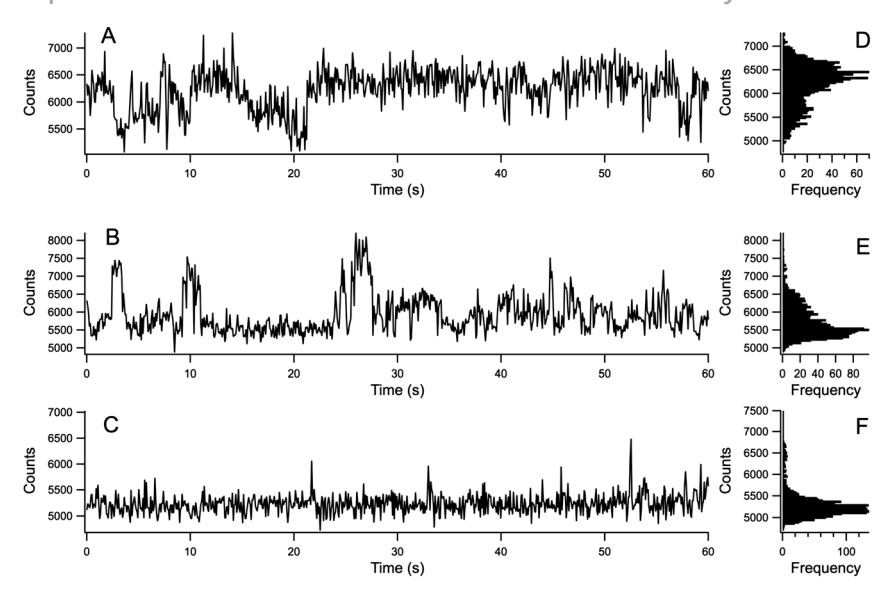


Fig. 3 Left: 60 s long fluorescence trajectories at applied potentials of (A) -0.2 V; (B) -0.48 V; (C) -0.8 VV. Each point in the trajectory is a 50 ms integration acquired at 82 ms intervals. Right: Intensity histograms for the full 150 s acquisition at applied potentials of (D) -0.2 V; (E) -0.48 V; (F) -0.8 V.

FAD molecule. Were multiple molecules responsible, the trajectory would exhibit a variable number of intensity states, depending on the number of molecules, with measurable activity at the intermediate levels. Because the digital fluorescence trajectories observed in the absence of applied potential have completely different dynamics (vide supra), the single FAD fluorescence transitions are clearly related to electrode potential and, thus, to electron transfer events.

Fig. 4 shows the distribution of fluorescence intensities for three separate single FAD molecules at each of three potentials (-0.2 V, -0.48 V, -0.8 V vs. Ag/AgCl), chosen to bracket E_{eq} . At each potential, the molecules show behavior which is qualitatively similar, but the details of the distributions differ. In contrast, the behavior is distinctly different at the three different potentials, with the weight of the distributions shifting from mostly 'on' at -0.2 V to mostly 'off' at -0.8 V, with molecules displaying a distribution weighted between the two states near the macroscopic E_{eq} value. Differences in the intensity distributions are observed among individual single FAD molecules at the same potential, i.e. different single FAD molecules in different ZMW nanopores, which could arise from a number of possible sources. Most directly, E_{eq} is certainly expected to vary from molecule to molecule, reflecting variations in bonding, steric issues and the local nature of the electrode.37

Starting at the most anodic potential, -0.2 V vs. Ag/AgCl, the behavior for which is displayed in Fig. 4(A)-(C), molecules represented in Fig. 4(A) and (B) are clearly dominated by a preponderance of on-state behavior, as would be expected from the macroscopic electrochemistry of the FAD cofactor. In contrast, the molecule in Fig. 4(C) shows a larger fraction of off-state, suggesting that the local $E_{\rm eq}$ for this molecule is shifted positive relative to the macroscopic average value.

When the applied potential is near the macroscopic $E_{eq} = -0.48 \text{ V}$, Fig. 4(D)–(F), the distributions are shifted to a larger fraction of off-times, as expected at this

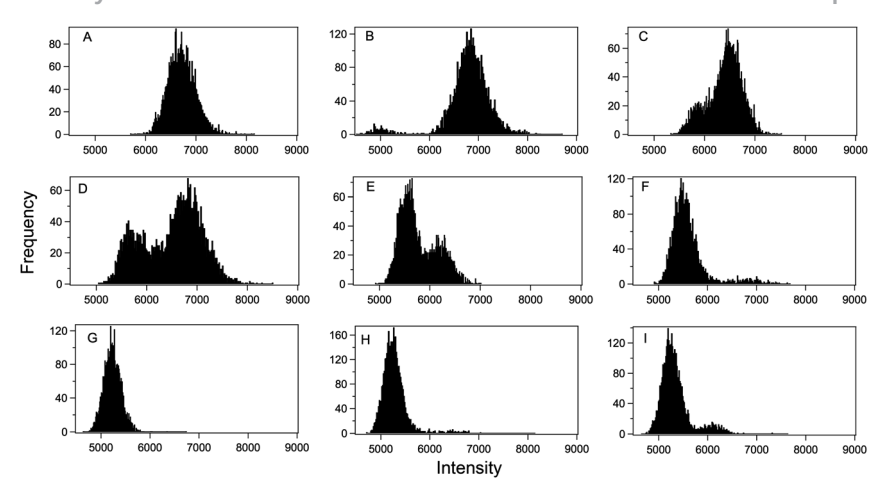


Fig. 4 Histograms of single molecule intensity distributions from 6 min trajectories for three representative molecules at each of three potentials. (A)–(C) -0.2 V; (D)–(F) -0.48 V; (G)–(I) -0.8 V. All potentials vs. Ag/AgCl reference.

more cathodic potential. Here, too, there are significant molecule-to-molecule differences consistent with local variations in $E_{\rm eq}$, cf. Fig. 4(D) and 4(F). At -0.8 V, Fig. 4(G)–(I), the fraction of on-times in the distributions are negligible, except for the molecule in Fig. 4(I) where it is small but measurable. These observations, taken collectively, are consistent with the macroscopic behavior in which oxidized FAD (predominant at -0.2 V) is luminescent, while reduced FADH₂ (the dominant species at -0.8 V) is dark. To further illustrate potential control over electron transfer to single FAD molecules immobilized in ZMWs, histograms of fluorescence intensity over tens of ZMW spots were analyzed at multiple potentials. Just as the results for the three specific molecules in Fig. 3 indicate, the distribution of fluorescence intensity shifts from levels consistent with a single molecule in the on-state to an off-state level at more cathodic applied potentials.

In addition to the fluorescence intensity distributions, the rate of on \rightarrow off and off \rightarrow on transitions also changes with applied potential. At cathodic (anodic) potential, the intensity distributions indicate molecules in the off (on) state, and as can be seen in Fig. 3, transitions between levels are infrequent and the duration in the opposite state is short. However, as is evident in Fig. 3, the rate of transitions is larger near $E_{\rm eq}$. Transition rates at specified potentials were obtained by fitting the histogram of on-time and off-time distributions. In one particularly long (10 min observation time) but otherwise representative fluorescence trajectory, obtained at $E_{\rm eq} = -0.48$ V vs. Ag/AgCl, both on-time and off-time distributions exhibited single exponential decay with approximately the same decay constant, $k_{\rm on} \approx k_{\rm off} \approx 2.5~{\rm s}^{-1}$, consistent with the reduction rate and the oxidation rate being comparable to each other near $E_{\rm eq}$.

Potential dependence

We hypothesize that the probability of electron transfer is potential-dependent on a single molecule basis. The probability of observing a reduced state (p_{red}) should

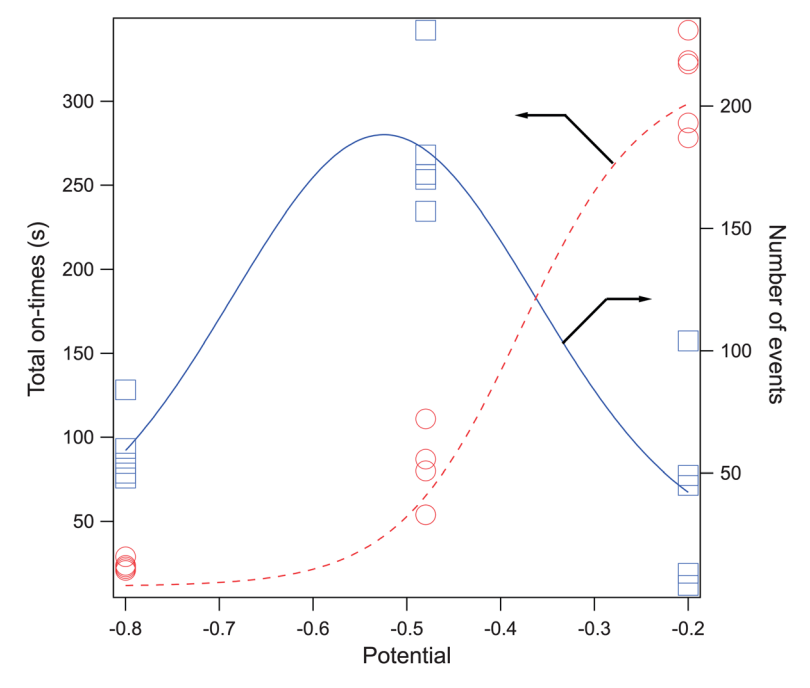


Fig. 5 Potential dependence of total on-time duration (left, red, circles) and the number of transition events (right, blue, squares) for 15 separate 6-min trajectories; 5 at each potential. The total on-time duration and number of transitions are fit to sigmoid (red, dashed) and Gaussian (blue, solid) functions, respectively.

approach 1 as the potential is scanned negative of E_{eq} , and similarly, the probability of observing an oxidized state (p_{ox}) should approach 1 as the potential is scanned positive of E_{eq} . Because the observed transition rate depends on having non-zero probabilities for both $p_{\rm red}$ and $p_{\rm ox}$, the maximum should be reached near $E_{\rm eq}$, falling off to either side, so the transition rate is expected to be a maximum when the potential is held near the ensemble-averaged value of $E_{\rm eq}$. Comparison of the fluorescence trajectories of single FAD molecules at different potentials in Fig. 3 clearly indicates that the rate at which transitions between FAD and FADH₂ occur is potential dependent. Consistent with this hypothesis, Fig. 5 shows that the total on-time duration increases with increasingly anodic applied potential. In addition, Fig. 5 indicates that the rate at which transitions between luminescent (oxidized, FAD) and dark (reduced, FADH₂) states occur can be modulated with electrochemical potential, with the maximum rate occurring near E_{eq} . The curve is symmetric around E_{eq} , and consistent with expectations, the transition frequency is a maximum at E_{eq} .

Conclusions

We have explored the possibility of using electrochemically-active zero-mode waveguides to examine potential-dependent blinking behavior of single FAD/ FADH₂ molecules covalently immobilized to the Au cladding layer of the ZMW. The optical fields are not as well-confined in Au-clad ZMWs as in those with Al cladding, but the small difference is compensated by access to Au self-assembly chemistry, which is used here to fashion a molecular wire construct utilizing an intermediate PQQ linker. The efficacy of this linker strategy is well-demonstrated by the single molecule electrochemical results. Fluorescence temporal trajectories and intensity distributions clearly indicate molecule-to-molecule variations in behavior at the same nominal potential, likely illustrating variations in local E_{eq} that may reflect, among other things, variations in bonding, steric constraints and the local nature of the electrode. Despite these individual differences, characterization of several tens of molecules at each potential show definite potentialdependent behavior: (1) the weight of the fluorescence intensity distributions shifts from mostly 'on' at -0.2 V to mostly 'off' at -0.8 V, with molecules displaying a distribution weighted between the two states near the macroscopic E_{eq} value; and (2) the rate of on \rightarrow off and off \rightarrow on transitions also changes with applied potential, reaching a maximum near E_{eq} . These observations are consistent with behavior expected for single electron transfer events. Using the dark ↔ emissive transition as an indicator of the FADH₂ ↔ FAD 2-electron redox process, strongly supports an interpretation of single redox events. The fluorescence intensity distributions scale with applied potential in exactly the same way as expected for the single molecule probabilities, p_{ox} and p_{red} . In addition, using a Fermi's Golden Rule formalism leads to the prediction that the rate of reduction reactions, for example, should scale with the probability that the molecule is initially oxidized, *i.e.* $p_{ox} = 1 - p_{red}$. This, in turn, predicts that the transition rate should be largest near E_{eq} , exactly as observed.

Given the success of these potential-controlled ZMW-immobilized single molecule spectroelectrochemistry experiments, we anticipate further exploiting this capacity to modulate the quantum efficiency of a redox-sensitive fluorophore by immobilizing single copies of FAD-containing redox-active flavoenzymes in order to explore individual electron transfer events at single enzyme molecules. In these single enzyme spectroelectrochemistry experiments, we expect to see even more dramatic molecule-to-molecule differences given the structure (surface orientation) dependent efficiency of electron transfer.

Acknowledgements

This work was supported by the National Science Foundation through the Center for Nanoscale Chemical-Electrical-Mechanical Manufacturing Systems (JZ) and grant 1111739 (LPZ). Fabrication of ZMW electrode arrays was partially supported by the Notre Dame Integrated Imaging Facility and the Notre Dame Nanofabrication Facility, and development of the ZMW structures was funded by the Department of Energy through DE FG02 ER0715851.

References

- 1 L. Homchaudhuri, N. Sarma and R. Swaminathan, Biopolymers, 2006, 83, 477-486.
- 2 M. Jiang and Z. H. Guo, J. Am. Chem. Soc., 2007, 129, 730-731.
- 3 N. Kozer, Y. Y. Kuttner, G. Haran and G. Schreiber, Biophys. J., 2007, 92, 2139-2149.
- 4 N. Kozer and G. Schreiber, J. Mol. Biol., 2004, 336, 763-774.
- 5 Y. Y. Kuttner, N. Kozer, E. Segal, G. Schreiber and G. Haran, J. Am. Chem. Soc., 2005, 127, 15138-15144.
- 6 S. Zorrilla, M. A. Hink, A. J. W. G. Visser and M. P. Lillo, Biophys. Chem., 2007, 125, 298-305.

- 7 S. Zorrilla, G. Rivas, A. U. Acuna and M. P. Lillo, Protein Sci., 2004, 13, 2960-2969.
- 8 M. Levene, J. Korlach, S. Turner, M. Foquet, H. Craighead and W. W. Webb, Science, 2003, 299, 682-686.
- 9 J. M. Moran-Mirabal and H. G. Craighead, Methods, 2008, 46, 11-17.
- 10 J. M. Moran-Mirabal, A. J. Torres, K. Samiee, B. Baird and H. Craighead, Nanotechnology, 2007, 18, 195101.
- 11 K. T. Samiee, J. M. Moran-Mirabal, Y. K. Cheung and H. Craighead, Biophys. I., 2006, 90, 3288-3299.
- 12 M. Foquet, K. Samiee, X. Kong, B. P. Chauduri, P. Lundquist, S. Turner, J. Freudenthal and D. B. Roitman, J. Appl. Phys., 2008, 103, 034301.
- 13 J. Korlach, P. J. Marks, R. L. Cicero, J. J. Gray, D. L. Murphy, D. B. Roitman, T. T. Pham, G. A. Otto, M. Foquet and S. Turner, Proc. Natl. Acad. Sci. U. S. A., 2008, 105, 1176-1181.
- 14 J. Eid, A. Fehr, J. Gray, K. Luong, J. Lyle, G. Otto, P. Peluso, D. Rank, P. Baybayan, B. Bettman, A. Bibillo, K. Bjornson, B. Chaudhuri, F. Christians, R. Cicero, S. Clark, R. Dalal, A. Dewinter, J. Dixon, M. Foquet, A. Gaertner, P. Hardenbol, C. Heiner, K. Hester, D. Holden, G. Kearns, X. X. Kong, R. Kuse, Y. Lacroix, S. Lin, P. Lundquist, C. C. Ma, P. Marks, M. Maxham, D. Murphy, I. Park, T. Pham, M. Phillips, J. Roy, R. Sebra, G. Shen, J. Sorenson, A. Tomaney, K. Travers, M. Trulson, J. Vieceli, J. Wegener, D. Wu, A. Yang, D. Zaccarin, P. Zhao, F. Zhong, J. Korlach and S. Turner, Science, 2009, 323, 133-138.
- 15 T. Miyake, T. Tanii, H. Sonobe, R. Akahori, N. Shimamoto, T. Ueno, T. Funatsu and I. Ohdomari, Anal. Chem., 2008, 80, 6018-6022.
- 16 J. B. Edel, M. Wu, B. Baird and H. Craighead, Biophys. J., 2005, 88, L43-L45.
- 17 J. Wenger, D. Gerard, P.-F. Lenne, H. Rigneault, J. Dintinger, T. W. Ebbesen, A. Boned, F. Conchonaud and D. Marguet, Opt. Express, 2006, 14, 12206-12216.
- 18 J. Zhao, S. P. Branagan and P. W. Bohn, Appl. Spectrosc., 2012, 66, 163-169.
- 19 M. Pita and E. Katz, J. Am. Chem. Soc., 2008, 130, 36-37.
- 20 F. R. F. Fan and A. J. Bard, Science, 1995, 267, 871-874.
- 21 F. R. F. Fan, J. Kwak and A. J. Bard, J. Am. Chem. Soc., 1996, 118, 9669-9675.
- 22 A. J. Bard, ACS Nano, 2008, 2, 2437-2440.
- 23 F. J. M. Hoeben, F. S. Meijer, C. Dekker, S. P. J. Albracht, H. A. Heering and S. G. Lemay, ACS Nano, 2008, 2, 2497-2504.
- 24 W. E. Moerner and D. P. Fromm, Rev. Sci. Instrum., 2003, 74, 3597–3619.
- 25 H. Park, G. T. Hanson, S. R. Duff and P. R. Selvin, J. Microsc., 2004, 216, 199-205.
- 26 E. Cortes, P. G. Etchegoin, E. C. Le Ru, A. Fainstein, M. E. Vela and R. C. Salvarezza, J. Am. Chem. Soc., 2010, 132, 18034-18037.
- 27 C. H. Lei, D. H. Hu and E. J. Ackerman, *Chem. Commun.*, 2008, 5490–5492.
- 28 R. E. Palacios, F. R. F. Fan, A. J. Bard and P. F. Barbara, J. Am. Chem. Soc., 2006, 128, 9028-9029.
- 29 C. H. Lei, D. H. Hu and E. Ackerman, Nano Lett., 2009, 9, 655-658.
- 30 H. Lu, L. Xun and X. Xie, Science, 1998, 282, 1877-1882.
- 31 W. Min, I. V. Gopich, B. P. English, S. C. Kou, X. S. Xie and A. Szabo, J. Phys. Chem. B, 2006, 110, 20093-20097.
- 32 A. Tyagi and A. Penzkofer, J. Photochem. Photobiol., A, 2010, 215, 108-117.
- 33 W. P. Ambrose, P. M. Goodwin, J. H. Jett, A. Van Orden, J. H. Werner and R. A. Keller, Chem. Rev., 1999, 99, 2929-2956.
- 34 J. C. Fister, S. C. Jacobson, L. M. Davis and J. M. Ramsey, Anal. Chem., 1998, 70, 431-437.
- 35 S. T. Plummer, P. W. Bohn, R. A. Stockton and M. A. Schwartz, Langmuir, 2003, 19, 7528-
- 36 O. Wang and P. W. Bohn, J. Phys. Chem. B, 2003, 107, 12578–12584.
- 37 G. K. Rowe, M. T. Carter, J. N. Richardson and R. W. Murray, Langmuir, 1995, 11, 1797-1806.